Dynamics Simulation of Self-assembly of Disc-like Nanoparticles

Bo Du

China Institute of Building Standard Design & Research Co., Ltd., Beijing, China

dubo2008@tju.edu.cn

Abstract. Brownian dynamics of self-assembly of disklike nanoparticles is simulated with a generalized aspherical model using tabulated method of force field parameters. The present model uses the force field of all-atom objects using tabulated table parameters which inherently reflects the specification of shape and component of nanoparticle. We study the self-assembly of disc-like particles. The transition mechanism is analyzed and discussed.

Keywords: nanoparticles, self-assemble, Brownian dynamics simulation.

1. Introduction

Nanoparticles with different shapes can self-assemble into specific structures and these structures are of great interest in a wide variety of fields from materials science to biology fields [1]. For example, disc-like nanoparticles can self-assemble to a columnar structure, John et.al. [2] provide a process for the synthesis of nanoscale discotic liquid crystalline porphyrins. The materials may be used as photovoltaic materials, organic semiconductors, organic light emitting materials and photoresponsive semiconductor. Eugenia et.al. [3] report the assembly of superlattices of multicomponent nanorods (Au-tipped CdSe nanorods). The self-assembled structures of these nanoparticles are useful. How to control the formation of these structures is extremely important, and we are anxious to know the self-assembly mechanism of nanoparticles. In experiment, people determine the self-assembly process with the electron micrograph, dynamic light scattering, etc. However, these speculations would need further verify, we will use computer simulation methods to study the formation mechanism of different shapes of nanoparticles.

In this work, we present a generalized aspherical model using force field tabulated methods and show how it can be calculated effectively and parametrized in practical applications. Using this model, any axisymmetric particles can be constructed with the full conservation of particle specification via a pair potential. Also it can apply to non-identical molecules. On the other hand, such a potential would be quite useful, first for the possibility of modeling mixtures, which are often used in practical applications. Using this new algorithm, we studied disc-shaped nanoparticles. The aggregation process is clearly shown. The description of the model and the implementation of the simulation method for nanoparticles are presented in Secs. II. In Sec. III, the results of nanoparticles are analyzed and discussed. The conclusion remarks are given at the final part. Our method provide a simple way to explore the particle system and should possess broad application in simulation of various field such protein aggregation, virus building and nanoparticles design.

2. Model

2.1 Construction of anisotropic nanoparticles and target force field

The anisotropic nanoparticles are packed by the Van der Waals superatoms, as shown in Fig 1. Each nanoparticles consists of M interaction sites, or superatoms, positioned on a lattice shown in Fig. 1.

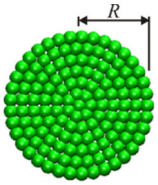


Fig. 1 The schemed of anisotropic nanoparticles.

Interaction sites or superatoms in different nanoparticles interact via the Lennard-Jones (LJ) 6-12 potential, and then the total potential energy is calculated as the sum over all such pair interactions. If the coordinates of two nanoparticles are denoted using the superscripts I and J, and the sites within each nanoparticles by subscripts i and j, then for site-site potentials the total energy is calculated by Eq.1[4].

$$U_{IJ} = \sum_{i\in I}\sum_{j\in J} U_{ij}^{IJ} = \sum_{i\in I}\sum_{j\in J} 4\varepsilon_0[(\frac{\sigma_0}{r_{ij}})^{12} - (\frac{\sigma_0}{r_{ij}})^{6}], \tag{1}$$

where U_{ij}^{IJ} is the pair potential between the sites *i* in particle *I* and *j* in particle *J*, ε_0 is the depth of the potential well, σ_0 is the (finite) distance at which the inter-particle potential is zero, and r_{ij} is the distance between the particles.

2.2 Extraction of force field of particle using tabulated method.

The template is used to format your paper and style the text.

We investigated a system of *N* nanoparticles of revolution interacting via a modified form of the GB pair potential, where each nanoparticles *I* has a single site representation, defined by the position $\boldsymbol{r}_I(x_I, y_I, z_I)$ of its center of mass in the laboratory frame and a unit vector $\boldsymbol{u}_I(u_{Ix}, u_{Iy}, u_{Iz})$ along the axis of symmetry in the height direction. The angle between $\boldsymbol{u}_I$ and $\boldsymbol{r}_{IJ}$ is α_I, the angle between $\boldsymbol{u}_J$ and $\boldsymbol{r}_{IJ}$ is α_J and the dihedral angle of $\boldsymbol{u}_I$, $\boldsymbol{r}_{IJ}$, $\boldsymbol{u}_J$ is β_{IJ}. The relationship between $\alpha_I, \alpha_J, \beta_{IJ}$ and $\boldsymbol{u}_I$, $\boldsymbol{r}_{IJ}$, $\boldsymbol{u}_J$ is shown in Eq.2.

$$\begin{aligned} \alpha_I &= \arccos(\boldsymbol{u}_I \cdot \hat{\boldsymbol{r}}_{IJ}), \alpha_J = \arccos(\boldsymbol{u}_J \cdot \hat{\boldsymbol{r}}_{IJ}), \\ \beta_{IJ} &= \arccos((\boldsymbol{u}_I \times \hat{\boldsymbol{r}}_{IJ}) \cdot (\boldsymbol{u}_J \times \hat{\boldsymbol{r}}_{IJ})), \end{aligned} \tag{2}$$

where $\alpha_I, \alpha_J, \beta_{IJ} \in [0, \pi]$, $\hat{\boldsymbol{r}}_{IJ} = \boldsymbol{r}_{IJ} / r_{IJ}$, "×" is responsible for cross product. Then the Gay-Berne potential function can be expressed as Eq.3.

$$U_{IJ} = 4\varepsilon(\alpha_I, \alpha_J, \beta_{IJ})\left[\left(\frac{\sigma(\alpha_I, \alpha_J, \beta_{IJ})}{r_{IJ} - \Delta r(\alpha_I, \alpha_J, \beta_{IJ})}\right)^{12} - \left(\frac{\sigma(\alpha_I, \alpha_J, \beta_{IJ})}{r_{IJ} - \Delta r(\alpha_I, \alpha_J, \beta_{IJ})}\right)^{6}\right] \tag{3}$$

where α, β, θ are the angles in degrees, U_{IJ} is the interaction between two nanoparticles *I* and *J*. The potential not only depends on the molecular shape parameter $\sigma(\alpha_I, \alpha_J, \beta_{IJ}), \Delta r(\alpha_I, \alpha_J, \beta_{IJ})$ but also on well depth parameter $\varepsilon(\alpha_I, \alpha_J, \beta_{IJ})$ through the anisotropic terms. The equilibrium distance $r_m = 2^{1/6}\sigma(\alpha_I, \alpha_J, \beta_{IJ}) + \Delta r(\alpha_I, \alpha_J, \beta_{IJ})$. Using three finite angles represent the potential, the conformation space can be easily visited. For full flexibility, potential interaction can be used for nanoparticles through user-supplied tabulated numerical potential. Then the setup of numerical tabulate potential is as follows: the state $\boldsymbol{u}_I = (0,0,1), \boldsymbol{r}_I = (0,0,0)$ is defined as essential state. The state of nanoparticle *I* is the essential state rotated α_I by *x* axis. The state of nanoparticle *J* is the essential state rotated α_J by *x* axis and then rotated β_{IJ} by *z* axis, and the $\boldsymbol{r}_I$ is changed into (0,0, r_{IJ}). Using Eq.1, the energy U_{IJ} is calculated with different distance r_{IJ}. The data $U_{IJ} \square r_{IJ}$ is used to fit the varied GB potential models shown in Equation (2). The energy fitting method is shown in Fig 1. The fitting line and the $U_{IJ} \square r_{IJ}$ line at least have two same points $U_{\min}(r_m)$ and $U(r_m + \square r)$.

Using dichotomy, we find the minister potential energy point $U_{\min}(r_m)$ in U_{IJ} □ r_{IJ}. The depth parameter $\varepsilon(\alpha_I,\alpha_J,\beta_{IJ})=-U_{\min}(r_m)$. And then we select two point $U_{\min}(r_m)$ and $U(r_m+$□$r)$ to solve equations. Then $\sigma(\alpha_I,\alpha_J,\beta_{IJ})$, $\Delta r(\alpha_I,\alpha_J,\beta_{IJ})$ and $\varepsilon(\alpha_I,\alpha_J,\beta_{IJ})$ are stored. The force routines get a table with these three parameters and an angle interval number N_{BIN} that is equal to the number of angle intervals per π. These three parameters are like a positional numeral system with a radix, or base, of π degrees; each parameter should go from 0 up to and including π degrees with the table spacing $h=\pi/N_{BIN}$.

However, in a free-energy calculation, using the simple interpolation of the version of the GB potentials as described in Equation (3) may lead to poor convergence. To scale the interaction function in a manner consistent with the soft-core form, the soft-core interaction is presented as shown in Equation (4).

$$U_{IJ}^{sc}=\begin{cases}[U_{\max}+\varepsilon(\alpha_I,\alpha_J,\beta_{IJ})](1-r_{IJ}/r_m)^2-\varepsilon(\alpha_I,\alpha_J,\beta_{IJ}), r_{IJ}<r_m\\ 4\varepsilon(\alpha_I,\alpha_J,\beta_{IJ})\left[\left(\frac{\sigma(\alpha_I,\alpha_J,\beta_{IJ})}{r_{IJ}-\Delta r(\alpha_I,\alpha_J,\beta_{IJ})}\right)^{12}-\left(\frac{\sigma(\alpha_I,\alpha_J,\beta_{IJ})}{r_{IJ}-\Delta r(\alpha_I,\alpha_J,\beta_{IJ})}\right)^{6}\right], r_{IJ}\geq r_m\end{cases} \tag{4}$$

where U_{max} is the potential energy at r_{IJ}=0. In order to ensure the potential energy curve is continuous, the r_m equals the equilibrium distance. Then when $r_{IJ}<r_m$, the potential energy is liked elastic repulsion potential. When $r_{IJ}\geq r_m$, the potential energy is the modified Gay-Berne potential. The zero energy contour surface around the disc shaped particle interacting with another parallel one has an essentially disc shape and it is convenient to think of particles interacting via the tabulated potentials simply as soft attractive-repulsive disc.

The effect of solvation is taken into account by frictional and random position acting on nanoparticles. Brownian dynamics (BD) simulations is proposed in Eq. (5).

$$\begin{aligned}\boldsymbol{v}_I(t+\Delta t)&=\frac{\boldsymbol{f}_I}{\gamma_I}+\sqrt{2k_BT\frac{r_I^G}{\Delta t\gamma_I}},\\ \boldsymbol{l}_I(t+\Delta t)&=\frac{\boldsymbol{I}\boldsymbol{\tau}_I}{\gamma_I^q}+\boldsymbol{I}\sqrt{2k_BT\frac{r_I^G}{\Delta t\gamma_I^q}},\end{aligned} \tag{5}$$

where Δt is the time step, $\boldsymbol{f}_I$ is the force, $\boldsymbol{\tau}_I$ is the torque, $\boldsymbol{l}_I$ is the angular momentum, k_B is the Boltzmann parameter, T is the temperature, r_I^G is Gaussian distributed noise with $\mu=0,\sigma=1$. The friction coefficient $\gamma_I=m_I/\xi_I$ can be chosen the same for all particles, where ξ_I is the friction constant. In the same way $\gamma_I^q=I^q/\xi_I^q$, where I^q is the moment of inertia. Because the system is assumed to be over-damped, large time steps can be used.

3. Results and Discussions

We have performed four series of BD simulations in NVT ensemble using samples of N particles with different shapes (discs) or different interaction anisotropies.

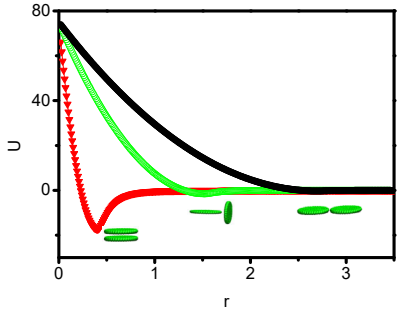


Fig. 2 The energy profiles correspond to different configurations for disc-shaped nanoparticles.

The disc-shaped nanoparticles are packed by 133 isotropic superatoms (with $N = 400$, $R = 1.1$ nm, $d_{max} = 0.2$ nm, $\sigma_0 = 0.4$ and $\varepsilon_0 = 0.2$), as shown in Fig. 1. The mass of nanoparticles is 1.33 and the moment of inertia $I = 1.02$. In Fig. 2 we show the energy profiles for disc-shaped nanoparticles, which correspond to different configurations. It is clear that the well depth of face-to-face configuration is largest. The cutoff for nonbonded interactions is $r_c = 3.5$ nm, and the friction coefficient $\gamma = 0.01$. The system is cooled from 200 to 10 K with a rare of $31.7\ \mathrm{K/\mu s}$. Long time Brownian MD simulations are performed out to collect enough trajectories for obtaining equilibrium distribution data. The simulation time is 6 μs with the time step 20 fs.

In order to characterize the phase behavior of the system the second-rank orientational order parameter P_2 [5-7] and the fourth-rank orientational order parameter P_4 [6, 8] are computed via:

$$S_{\alpha\beta} = \frac{1}{N}\sum_{i=1}^{N}\frac{1}{2}(3e_{i\alpha}e_{i\beta} - \delta_{\alpha\beta}), \tag{6}$$

where $\alpha, \beta = x, y, z$ are the indices referring to the laboratory frame, $\delta_{\alpha\beta}$ the Kronecker symbol, and <...> the ensemble average. The eigenvectors of $S_{\alpha\beta}$ give the preferred alignment directions and the eigenvalues give the degree of orientational ordering. [9] Herein, P_2 is the largest eigenvalue of the order parameter $S_{\alpha\beta}$

$$< P_4 >= \frac{35}{8} < \cos^4\beta > - \frac{30}{8} < \cos^2\beta > + \frac{3}{8}, \tag{7}$$

where $\cos\beta = \boldsymbol{u}\cdot\hat{\boldsymbol{n}}$, the director $\hat{\boldsymbol{n}}$ is the eigenvector corresponding to the P_2. The order parameter is a crucial factor in relating to experiment, since it determines the observed anisotropy in second/fourth rank tensor properties.

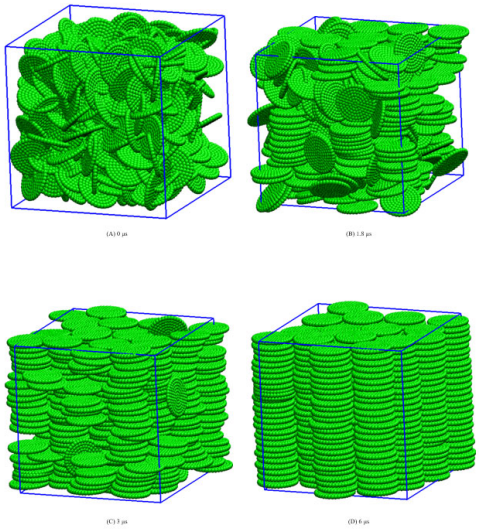


Fig. 3 The simulation of disc-shaped nanoparticles.

Even though the nematic phase is characterized by a substantial degree of orientational order the distribution of center-of-mass positions exhibits the typical short-range order characteristic of ordinary fluids where the typical correlation lengths are comparable to the range of intermolecular interactions. This changes in the smectic-A phase where molecules do not only align with $\hat{\boldsymbol{n}}$ but also develop long-range positional order, that is, they form individual layers in the direction of $\hat{\boldsymbol{n}}$. However, positional order remains short range in directions orthogonal to $\hat{\boldsymbol{n}}$ such that within a given layer the structure remains fluidlike. Because of the layering of the fluid in the direction of $\hat{\boldsymbol{n}}$ a suitable quantitative measure of smectic order is given by the leading coefficient of the Fourier transform of the local density $\rho(\boldsymbol{r}\cdot\hat{\boldsymbol{n}})$ [5]

$$\Lambda = \frac{1}{N}\left\langle \left| \sum_{j=1}^{N} \exp\left[\frac{2\pi i (\boldsymbol{r}_j \cdot \hat{\boldsymbol{n}})}{d} \right] \right| \right\rangle, \tag{8}$$

where d is the spacing between adjacent smectic-A layers. If these layers were ideal, $d = H/D$ (D=2R, see Sec. II A). However, in practice $d \geq H/D$ on account of thermal fluctuations. Hence, in each configuration $(\boldsymbol{r}_I, \boldsymbol{u}_I)$, d is adjusted such as to maximize Λ. From Equation (10) it is also apparent that $\Lambda \in [0,1]$. In the nematic phase the superposition of the complex exponential functions in Equation (11) causes $\Lambda \approx 0$ because in the direction of $\hat{\boldsymbol{n}}$ a periodic structural feature of periodicity d does not exist; by a similar token $\Lambda \approx 1$ in the smectic-A phase.

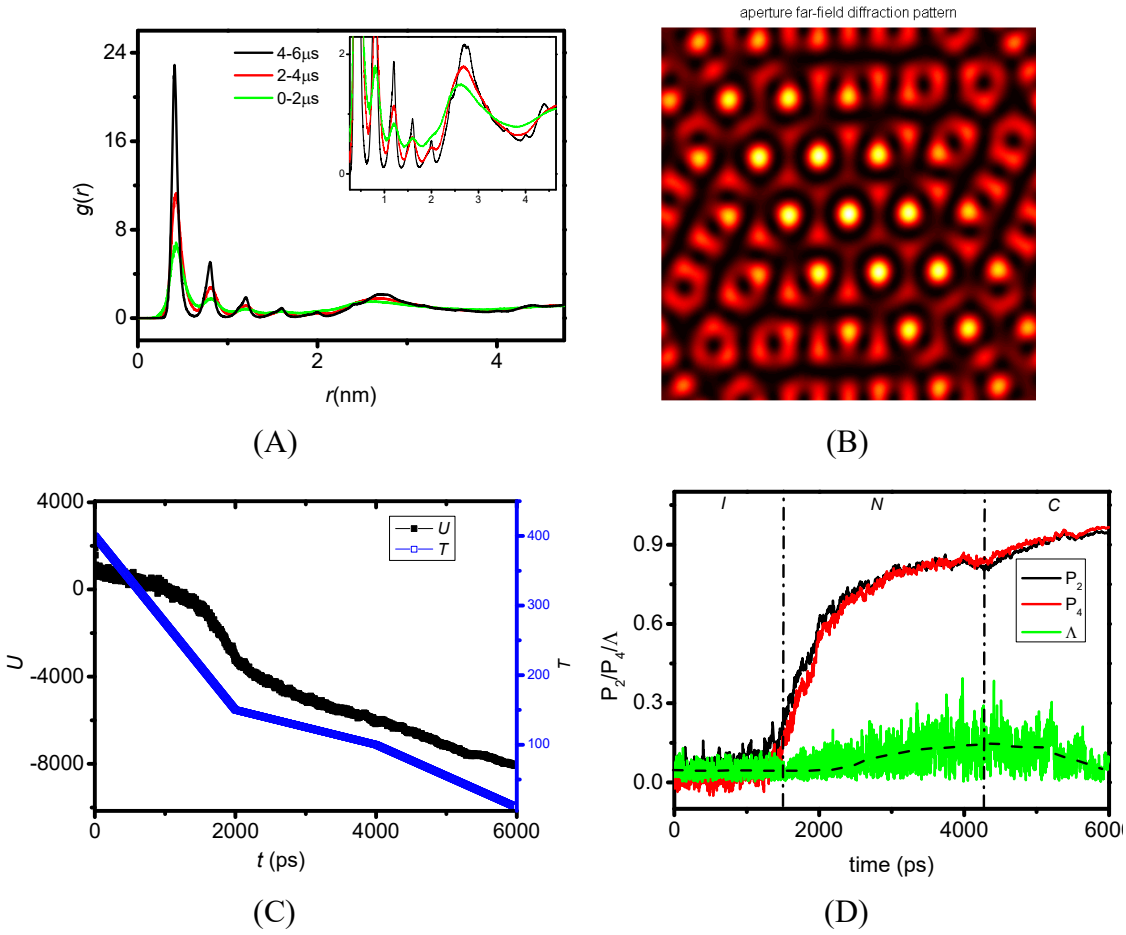


Fig. 4 Equilibrium for the disc-shaped nanoparticles: (A) The radial distribution function (RDF) of the centroid positions of the system, (B) The aperture far-field diffraction pattern of the equilibrium structure of the disc-shaped nanoparticles, (C) The total energy U of the system as a function of the simulation time and the reference temperatureas T of the system as a function of the simulation time, (D) The P_2 and P_4 of the system as a function of simulation time.

Fig. 4(D) shows P_2, P_4 and Λ as a function of the simulation time. Both P_2/P_4 and Λ are close to zero at high temperatures, identifying the isotropic (I) phase. Upon cooling P_2/P_4 jumps to an intermediate value, indicating a transition from the isotropic to the nematic phase (N). Further cooling results in a gradual increase of P_2/P_4 towards unity and a small decrease of Λ, followed by another discontinuity, suggesting a transition from the N phase to another (a columnar phase C).Examination of the translational structure through radial distribution functions confirms the occurrence of the transition. In Fig. 4(A), the distribution function $g(r)$ is shown at several representative temperature stages. Five peaks for $g(r)$ less than $5(\sigma_{ff} + \Delta r_{ff})$ ($\sigma_{ff} + \Delta r_{ff} \approx 0.4$, as is

shown in Fig. 2) with positional ratio close to 1:2:3:4:5 stand for the translational order along the molecular axis $r_{\parallel}$. The appearance of periodic structures in $g(r)$ implies column formation with periodic stacking of particles at an inter-nanoparticles separation of ~0.4. The other two peaks, especially for 4-6 μs, for $g(r)$ less than $\sqrt{3}(\sigma_{ee}+\Delta r_{ee})$ ($\sigma_{ee}+\Delta r_{ee}\approx 2.7$, as is shown in Fig. 2) with positional ratio close to $1:\sqrt{3}$ stand for the translational order along $r_{\perp}$ ($r_{\parallel}\perp r_{\perp}$). And Fig.4(B) shows the far-field diffraction pattern. These confirm hexagonal column packing. As can be seen in Fig. 4(a), the tendency for translational order along $r_{\parallel}$ grows stronger as the system is cooled below the *N*-*C* phase boundary.

To get a better feel for the structure of the system in the *I*, *N*, and *C* phases we present configuration in Fig.3. The typical features of the low temperature organisations clearly show a liquid crystalline structure formed by hexagonal columnar phases, induced by spatial ordering of the columnar axis and positional correlations between neighboring columns.

4. Conclusion

We have used Brownian Dynamics to investigate the self-assembly of different shaped nanoparticles with force field tabulated methods. It is found that it can be calculated effectively and the geometry of nanoparticles plays important role in their self-assembly characteristics. And any axisymmetric particles can be constructed with the full conservation of particle specification via a pair potential. Using this model, we studied disc-shaped nanoparticles. It is found that they have I phases at high temperature and ordered phases at lower. In addition, the N phases are often found during the phase transition from the I phases to the ordered phases. Actually, this work can provide a practical guide to geometry considerations when designing self-assembly of nanoscale systems and is applicable to a broad range of assembly processes. Related studies are on the way, and we hope to make this model to simulate particles of arbitrary shape via a pair potential.

References

[1] Sun, Y., Mayers, B., Xia, Y., Adv Mater 2003, 15, 641-646.
[2] Harden Jr, J., Jakli, A., Li, Q., Li, L., Google Patents 2007.
[3] Zhao, N., Liu, K., Greener, J., Nie, Z., Kumacheva, E., Nano Lett 2009, 9, 3077-3081.
[4] JE, J., Proceedings of the Royal Society London A 1924, 106, 463-477.
[5] Mazza, M. G., Greschek, M., Valiullin, R., Schoen, M., Phys Rev E 2011, 83, 51704.
[6] Chakrabarti, D., Wales, D. J., Phys Rev Lett 2008, 100, 127801.
[7] Prost, J., The physics of liquid crystals, Oxford University Press 1995.
[8] Zannoni, C., J Mater Chem 2001, 11, 2637-2646.
[9] Evans, D. J., Mol Phys 1981, 42, 1355-1365.